Volume 9 | Number 27 | 21 July 2018 | Pages 3697–3842

Polymer Chemistry

rsc.li/polymers

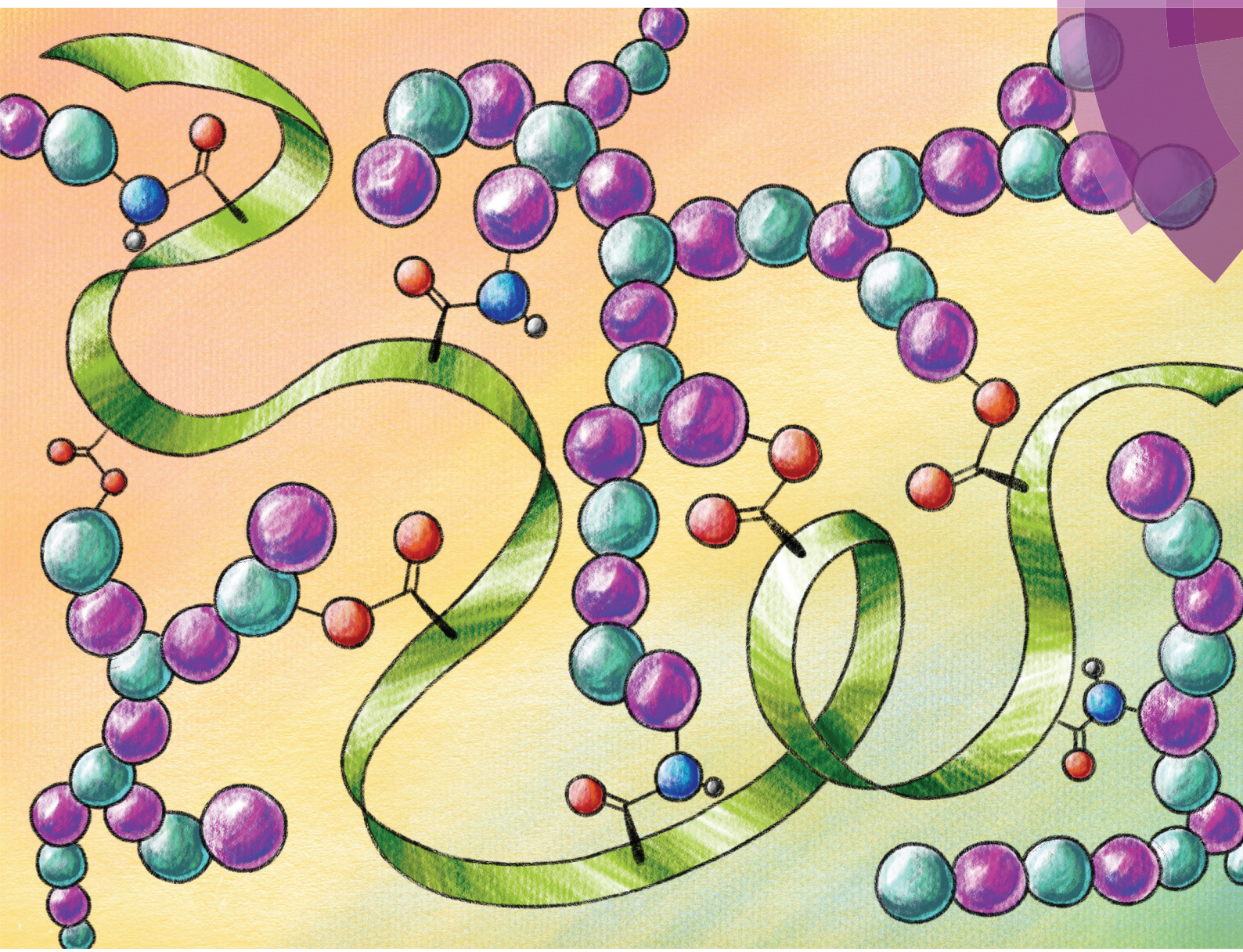

ISSN 1759-9962

ROYAL SOCIETY OF CHEMISTRY

PAPER

Sungkwon Yoon and Biqiong Chen

Elastomeric and pH-responsive hydrogels based on direct crosslinking of the poly(glycerol sebacate) pre-polymer and gelatin

Polymer Chemistry

The home for the most innovative and exciting polymer chemistry, with an emphasis on polymer synthesis and applications thereof

rsc.li/polymers

The Royal Society of Chemistry is the world's leading chemistry community. Through our high impact journals and publications we connect the world with the chemical sciences and invest the profits back into the chemistry community.

IN THIS ISSUE

ISSN 1759-9962 CODEN PCOHC2 9(27) 3697–3842 (2018)

Cover
See Sungkwon Yoon and Biqiong Chen, pp. 3727–3740.

Image reproduced by permission of Sungkwon Yoon from *Polym. Chem.*, 2018, **9**, 3727.

Inside cover
See Satyasankar Jana *et al.*, pp. 3741–3753.

Image reproduced by permission of Satyasankar Jana and Brendan Burkett from *Polym. Chem.*, 2018, **9**, 3741.

COMMUNICATIONS

3705

Inhibition of lysozyme's polymerization activity using a polymer structural mimic

D. L. Morris, T. C. Leeper* and C. J. Ziegler*

Hen egg white lysozyme (HEWL) is a green catalyst capable of polymerizing the formation of 2-ethynylpyridine. 1,3-di(2-pyridyl)propane (DPP) is a mimic of the polymer repeating unit and a polymerization inhibitor. DPP's interaction with HEWL reveals structural insight into the mechanism of polymerization.

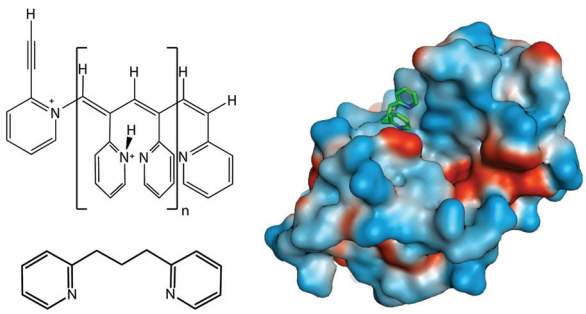

3709

Convenient synthesis of versatile syndiotactic polystyrene materials containing pendant alkenyl groups with a scandium catalyst system

Ke Yang, Hui Niu, Zhenghai Shi, Rui Tan, Tingting Li, Kaihua Shen and Yang Li*

The syndioselective copolymerization of styrene with five alkenyl functionalized styrenic monomers, with the use of a scandium catalyst, produced a new family of versatile syndiotactic polystyrene materials with pendant alkenyl groups.

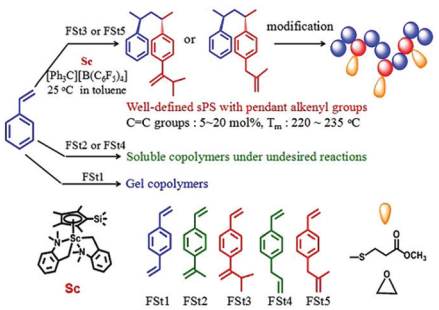

Editorial Staff

Executive Editor
Neil Hammond

Deputy Editor
Laura Fisher

Editorial Production Manager
Lucy Argyle

Development Editor
Garima Sharma

Senior Publishing Editor
Chris Goodall

Publishing Editors
Lorna Begley, Becky Dey, Laura Ghandhi, Chris Harding, Suzanne Howson

Editorial Assistant
Oliver Hill

Publishing Assistant
Allison Holloway

Publisher
Fiona McKenzie

For queries about submitted papers, please contact Lucy Argyle, Editorial Production Manager in the first instance. E-mail: **polymers@rsc.org**

For pre-submission queries please contact Neil Hammond, Executive Editor. E-mail **polymers-rsc@rsc.org**

Polymer Chemistry (electronic: ISSN 1759-9962) is published 48 times a year by the Royal Society of Chemistry, Thomas Graham House, Science Park, Milton Road, Cambridge, UK CB4 0WF.

All orders, with cheques made payable to the Royal Society of Chemistry, should be sent to the Royal Society of Chemistry Order Department, Royal Society of Chemistry, Thomas Graham House, Science Park, Milton Road, Cambridge, CB4 0WF, UK
Tel +44 (0)1223 432398; E-mail **orders@rsc.org**

2018 Annual (electronic) subscription price: £2417; $4128. Customers in Canada will be subject to a surcharge to cover GST. Customers in the EU subscribing to the electronic version only will be charged VAT.

If you take an institutional subscription to any Royal Society of Chemistry journal you are entitled to free, site-wide web access to that journal. You can arrange access via Internet Protocol (IP) address at **www.rsc.org/ip**

Customers should make payments by cheque in sterling payable on a UK clearing bank or in US dollars payable on a US clearing bank.

Polymer Chemistry

rsc.li/polymers

The home for the most innovative and exciting polymer chemistry, with an emphasis on polymer synthesis and applications thereof.

Editorial Board

Advisory Board

Information for Authors

Full details on how to submit material for publication in Polymer Chemistry are given in the Instructions for Authors (available from **http://www.rsc.org/authors**). Submissions should be made via the journal's homepage: **rsc.li/polymers**
Submissions: The journal welcomes submissions of manuscripts for publication as Full Papers, Communications, Perspectives and Reviews. Full Papers and Communications should describe original work of high quality and impact.

Colour figures are reproduced free of charge.
Additional details are available from the Editorial Office or **http://www.rsc.org/authors**

Registered charity number: 207890

COMMUNICATIONS

3714

CuAAC click chemistry: a versatile approach towards PVDF-based block copolymers

I. Terzic, N. L. Meereboer and K. Loos*

Functionalized benzoyl peroxide-initiated polymerization of vinylidene fluoride allows straightforward preparation of PVDF-based block copolymers with an appealing crystallization behavior.

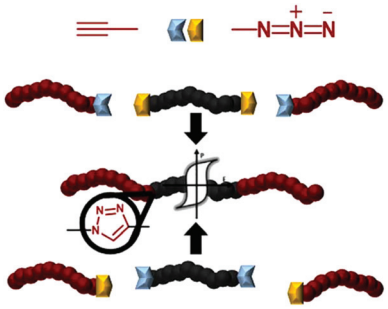

3721

Hydrogels with novel hydrolytically labile trehalose-based crosslinks: small changes – big differences in degradation behavior

Małgorzata Burek, Sylwia Waśkiewicz, Anna Lalik and Ilona Wandzik*

Novel crosslinkers based on trehalose diacetals were synthesized and applied to the fabrication of degradable polyacrylamide-type hydrogels with pH-dependent degradation characteristics at around physiological pH.

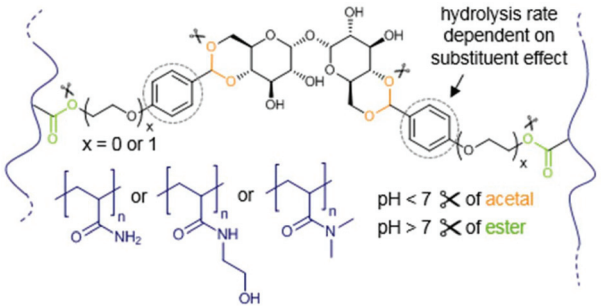

PAPERS

3727

Elastomeric and pH-responsive hydrogels based on direct crosslinking of the poly(glycerol sebacate) pre-polymer and gelatin

Sungkwon Yoon and Biqiong Chen*

The synthesis and biomedical applications of novel elastomeric, pH-responsive, biocompatible and biodegradable copolymer hydrogels based on poly(glycerol sebacate) and gelatin.

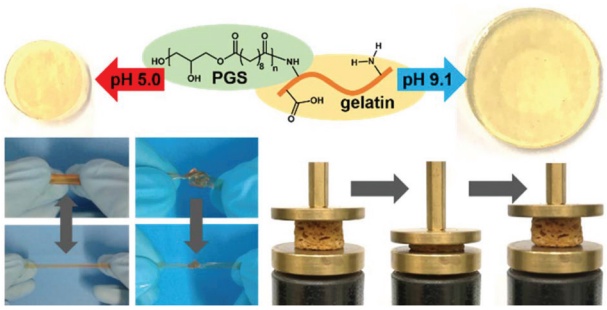

3741

Nucleophile-initiated anionic polymerization of zwitterionic monomers derived from vinylpyridines in aqueous media under ambient aerobic conditions

Satyasankar Jana,* Marco Klähn and Anbanandam Parthiban

Anionic polymerization of vinylpyridine based zwitterionic monomers using nucleophile initiators under natural conditions and DFT calculations for such polymerization are reported here.

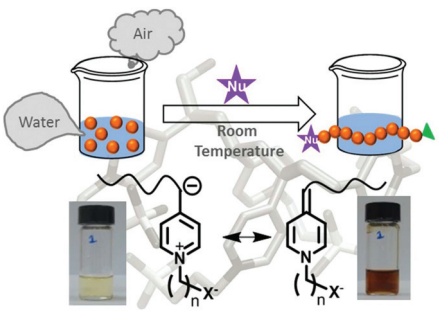

PAPERS

3754

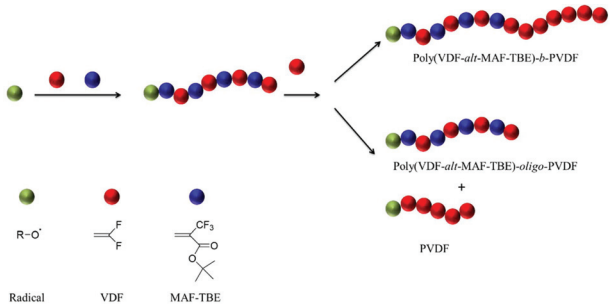

Kinetics of radical copolymerization of vinylidene fluoride with *tert*-butyl 2-trifluoromethyl acrylate: a suitable pair for the synthesis of alternating fluorinated copolymers

Panagiotis G. Falireas, Mohammad Wehbi, Ali Alaaeddine and Bruno Améduri*

A study of the copolymerization kinetics of vinylidene fluoride with *tert*-butyl 2-trifluoromethyl acrylate: a suitable pair for the synthesis of alternating fluorinated copolymers.

3762

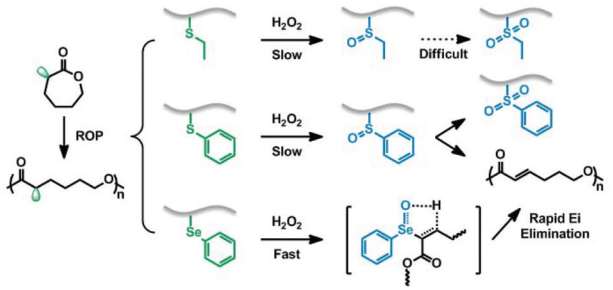

ROS-responsive poly(ε-caprolactone) with pendent thioether and selenide motifs

Li Yu, Mei Zhang, Fu-Sheng Du* and Zi-Chen Li*

Synthesis and oxidation properties of three chalcogen-containing ROS-responsive poly(ε-caprolactone)s have been reported.

3774

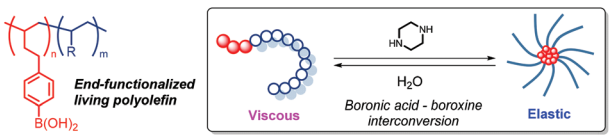

Reversible star assembly of polyolefins using interconversion between boroxine and boronic acid

Ryo Tanaka, Naoki Tonoko, Shin-ichi Kihara, Yuushou Nakayama and Takeshi Shiono*

The reversible star formation of polyolefins, with boronic acid modified chain-ends, was achieved.

3780

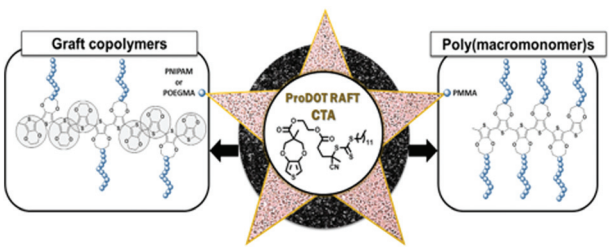

New electroactive macromonomers and multi-responsive PEDOT graft copolymers

Sara Marina, Daniele Mantione, Kasina ManojKumar, Vijayakrishna Kari, Junkal Gutierrez, Agnieszka Tercjak, Ana Sanchez-Sanchez* and David Mecerreyes*

Poly(3,4-ethylenedioxithiophene) (PEDOT) is the conducting polymer with the biggest prospects in the field of organic electronics due to its high electrical conductivity and transparency as thin films.

PAPERS

3791

Post-synthetic functionalization of a polysulfone scaffold with hydrazone-linked functionality

Dylan W. Domaille, Dillon M. Love, Xilal Y. Rima, Albert Harguindey, Benjamin D. Fairbanks, David Klug, Jennifer N. Cha and Christopher N. Bowman*

The synthesis, characterization, and post-synthetic functionalization of a readily functionalized step-growth linear polymer derived from divinyl sulfone (DVS) and *tert*-butylcarbazate (TBC) is presented.

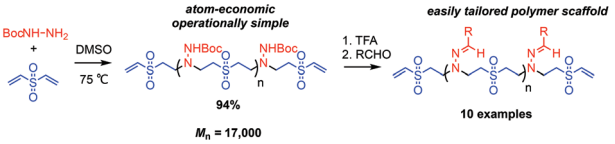

3798

Sustainable synthesis and characterization of a bisphenol A-free polycarbonate from a six-membered dicyclic carbonate

Pengrui Wang, Ji Hoon Park, Mahmoud Sayed, Tae-Sun Chang, Amy Moran, Shaochen Chen* and Sang-Hyun Pyo*

A BPA-free polycarbonate, a new type of highly thermally stable, optically transparent and biocompatible material was prepared from a di-cyclic carbonate.

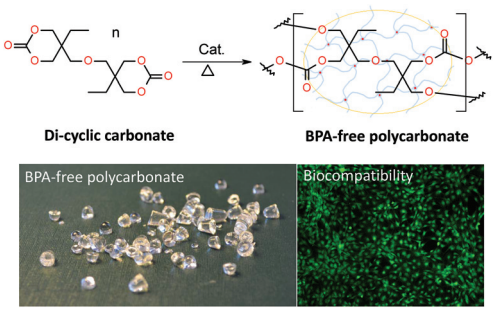

3808

A facile route to bespoke macro- and mesoporous block copolymer microparticles

Guping He, Thomas M. Bennett, Mohammad Alauhdin, Michael W. Fay, Xin Liu, Simon T. Schwab, Cheng-gong Sun and Steven M. Howdle*

A facile and versatile strategy to fabricate macro- and mesoporous block copolymer microparticles with bespoke characteristics using supercritical CO_2.

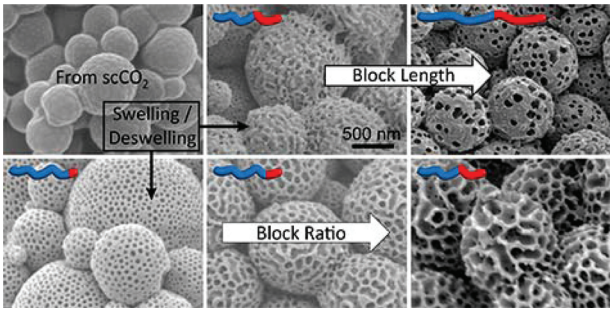

3820

Unraveling the stress effects on the optical properties of stretchable rod-coil polyfluorene-poly(*n*-butyl acrylate) block copolymer thin films

Hui-Ching Hsieh, Chih-Chien Hung, Kodai Watanabe, Jung-Yao Chen, Yu-Cheng Chiu, Takuya Isono, Yun-Chi Chiang, Renji R. Reghu, Toshifumi Satoh* and Wen-Chang Chen*

Novel deformable and fluorescent PF-*b*-PBA copolymers with nanofibrillar structures were synthesized for unraveling strain-dependent optical properties.

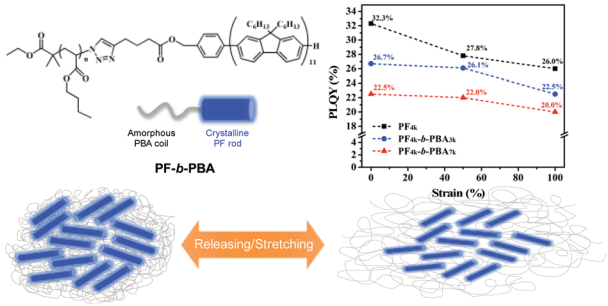

3832

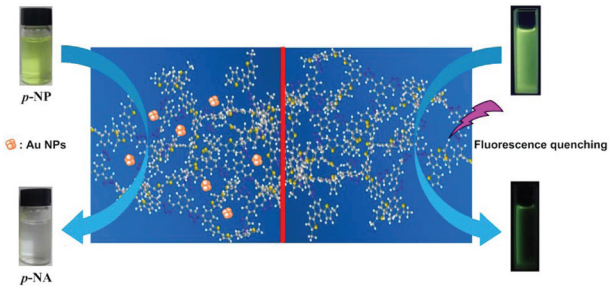

A 1,2,3-triazolyl based conjugated microporous polymer for sensitive detection of *p*-nitroaniline and Au nanoparticle immobilization

Feng Wei, Xinyi Cai, Junqi Nie,* Feiyi Wang, Cuifen Lu, Guichun Yang, Zuxing Chen, Chao Ma and Yuexing Zhang*

A 1,2,3-triazolyl based fluorescent CMP was used as an excellent chemosensor for *p*-nitroaniline detection and a support for Au catalyst deposition.

Polymer Chemistry

PAPER

View Article Online
View Journal | View Issue

Cite this: *Polym. Chem.*, 2018, **9**, 3808

A facile route to bespoke macro- and mesoporous block copolymer microparticles†

Guping He,[a] Thomas M. Bennett,[a] Mohammad Alauhdin,[a] Michael W. Fay,[b] Xin Liu,[c] Simon T. Schwab,[a] Cheng-gong Sun[c] and Steven M. Howdle*[a]

Received 8th May 2018,
Accepted 14th June 2018

DOI: 10.1039/c8py00707a

rsc.li/polymers

We report a facile and versatile strategy for the bespoke fabrication of macro- and mesoporous block copolymer microparticles. A clean synthetic route, RAFT dispersion polymerisation in supercritical carbon dioxide ($scCO_2$), is used to generate block copolymer microparticles. Selective swelling/deswelling is then applied to induce controlled morphology transitions and to trap the resulting porous state. The pore sizes are controllable over a large size range (~20–200 nm) by varying the length of the swellable block. Through a systematic approach we then demonstrate that the shape of the pores can also be tailored from isolated spheres through to interconnected/bicontinuous channels by varying the ratio of the two blocks. This process is shown to be applicable to a range of poly(methyl methacrylate) (PMMA)-based block copolymer systems, including PMMA-*b*-poly(4-vinyl pyridine), PMMA-*b*-poly(dimethyl acrylamide) (DMA) and PMMA-*b*-poly(dimethylaminoethylmethacrylate) (DMAEMA). In each case, the second minority block (*e.g.* P4VP, *etc.*) was selectively swollen with an alcohol to induce an order-to-order morphology transition and then quenched rapidly by the non-solvent hexane. This not only takes place on the order of hours, but is also freely scalable for the production of grams of material and beyond in a single step following polymerisation.

1. Introduction

Porous polymer particles have attracted significant attention because of their potential applicability to mainstream applications such as ion-exchange resins,[1,2] catalytic supports,[3–7] chromatography column materials,[8,9] and as solid supports for organic synthesis.[10,11] Additionally, there are potentially important emerging applications as templates for materials synthesis,[12,13] scaffolds for tissue engineering,[14–16] or as microsensors[17,18] and microreactors.[19–22] The key problem is that there is no simple scalable route to synthesise nanoporous microparticulate polymer materials with tunable dimensions across both length scales.

Block copolymers (BCPs) have been extensively exploited for the preparation of porous materials with well-defined nanopores.[23–28] Owing to the thermodynamic incompatibility of homopolymer chains, microphase separation occurs to yield periodic domains typically on the scale of 10–100 nm. These are well understood and give characteristic morphologies such as spheres, cylinders, gyroids, and lamellae.[29–32]

The traditional approach to create porous BCPs is to etch away one block to create voids.[33] Nanoporous polymers generated in this way can be exploited as templates for the formation of other nanostructured materials, for example *via* sol–gel methods.[25] The templated materials published so far have pore dimensions ranging from a few to 50 nm and up until now this has largely been achieved in 2D thin films of up to 500 nm in thickness. However, the process can be tedious and only a very limited range of BCPs with labile blocks have been devised for such purposes; for example, BCPs containing poly(methyl methacrylate) (PMMA),[34,35] polylactide,[36,37] and polymers with double bonds, *e.g.*, polybutadiene or polyisoprene,[38,39] which can be etched away by short-wave UV light exposure, hydrolysis and ozonolysis respectively.

A more recent and simpler approach uses solvent swelling/deswelling and evaporation to generate porosity without the need for sample degradation. The first reports were made on two dimensional (2D) micellar thin films[40] comprised of various amphiphilic BCPs such as PS-*b*-PAA[41–44] and polystyrene-*b*-poly(*x*-vinyl pyridine) (PS-*b*-P*x*VP, $x = 2$[45–48] or 4).[49–51] The polar solvents quickly penetrate the thin layers of the minority blocks, causing the micelle cores to undergo swelling that is confined within the continuous phase, while the majority blocks remain in a glassy state. Upon drying, the swollen core-

[a]*School of Chemistry, University of Nottingham, Nottingham, NG7 2RD, UK. E-mail: steve.howdle@nottingham.ac.uk*
[b]*Nanoscale and Microscale Research Centre, University of Nottingham, Nottingham, NG7 2RD, UK*
[c]*Faculty of Engineering, University of Nottingham, Nottingham, NG7 2RD, UK*

†Electronic supplementary information (ESI) available: Detailed BCP characteristics, GPC traces and SEM and TEM images of the original BCP microparticles before and/or after swelling. Tilt TEM videos demonstrating the fully porous nature of the five porous microparticle samples and their corresponding surface area and porosity properties. See DOI: 10.1039/c8py00707a

forming chains collapse on the surface of the non-swollen matrix and leave pores centred around the original location of the micelles, hence this method is called "confined swelling-induced pore generation".[44,52]

The same swelling induced porosity strategy has also been successfully utilised for so called one-dimensional (1D) BCP materials such as nanorods and nanofibers.[46,53–57] An additional template of anodic aluminium oxide (AAO) was used to produce nanorods (*ca.* 500 nm) that were then subjected to swelling in a selective solvent, such as ethanol for PS-*b*-P2VP. Compared to 2D thin films, which are confined to a solid substrate on one-side, the nanorods/nanofibers show morphology reconstruction in all directions.[46,54] Moreover, the pores are formed with an internal homogeneous wall/shell structure from the collapsed chains of the minority domains of the BCP. The pore structures were found to depend on the swelling agent, swelling temperature, swelling time, and BCP architecture.[46,58,59] The pore sizes were all <50 nm and the film thickness was limited to about 500 nm. Furthermore, Mei *et al.* were the first to demonstrate that AAO templates can also be used to produce nanoparticles with various internal nanoscale morphologies, including pores and layers, by varying the length of the swellable block.[60] Porosity was then introduced into these structures *via* the same solvent swelling approach.

Another related approach for creating porous nanoparticles is to use BCP solutions to create micelles *via* precipitation and then to apply a swelling/deswelling process where appropriate. This approach has also been shown to impart control of the pore size, shape and/or the overall particle diameter by varying the properties of the block copolymer used.[61,62] The limitation of this route is that the nanoparticle synthesis requires a slow and controlled precipitation and then evaporation from very dilute solutions (~1 wt%), a process that cannot easily be scaled to the gram or kilogram scale production of material.

Previously, we reported RAFT controlled dispersion polymerisation in $scCO_2$ as a unique route to create multigram quantities of microparticulate block copolymers.[63–65] Moreover, we have also demonstrated that the sizes of the microparticles can be controlled reproducibly from 300 nm through to 5.3 μm.[66] In this paper we exploit these novel BCP structures to create unique nanoporous microparticles from various systems including PMMA-*b*-P4VP, PMMA-*b*-PDMA and PMMA-*b*-PDMAEMA with controllable porosity over an unprecedented size range (10 nm to *ca.* 200 nm). Our methodology exploits synthesis in $scCO_2$ followed by a rapid alcohol based swelling induced morphology reconstruction of the minor block to create voids. To the best of our knowledge, this is the first time nanoporous microparticles with completely bespoke physico-chemical properties have been produced by a method that is realistically scalable.

2. Experimental section

2.1 Materials

Methyl methacrylate (MMA, Fisher, >99%), 4-vinylpyridine (4VP, Acros, 99%), dimethyl acrylamide (DMA, Aldrich, 99%), and dimethylaminoethylmethacrylate (DMAEMA, Aldrich, 99%) were purified by passing through a neutral alumina column and stored at −20 °C. 2-(Dodecylthiocarbonothioylthio)-2-methylpropionic acid (DDMAT) was synthesised following a literature procedure.[67] α-Azobis(isobutyronitrile) (AIBN, Wako, 97%) was purified by recrystallisation in ethanol. The dispersion stabiliser poly(dimethylsiloxane)-monomethyl methacrylate (PDMS-MA, ABCR, M_n = 10 000 g mol^{-1}), $CDCl_3$ (Aldrich, 99.9%), HPLC grade THF (Acros), chloroform (Aldrich, 99.9%), triethylamine (Acros, 99.9%) and iodine (Fisher) were used as received. Ruthenium tetroxide solutions were freshly prepared by mixing 12.4 mg of ruthenium chloride ($RuCl_3$, Aldrich, 99.9%) and 4.2 mg of sodium periodate ($NaIO_4$, Aldrich, 99.9%) in 1 ml deionized H_2O solution at 0 °C prior to use. Agar 100 resin (Agar Scientific) was used as received, and a formulation of medium hardness was used for embedding samples.

2.2 Synthesis of BCP microparticles *via* RAFT controlled dispersion in $scCO_2$

The synthesis of BCP microparticles followed earlier published procedures.[63,64] A typical one-pot synthesis is described below for $PMMA_{50}$-*b*-$P4VP_{33}$ where the subscripts denote the target MW in kg mol^{-1}. A high-pressure autoclave (60 ml) was flushed with CO_2 (5 MPa) for 15 min before adding the reactants for the synthesis of the first block. MMA (7.5 g), DDMAT RAFT agent (55 mg), AIBN initiator (25 mg), and PDMS-MA surfactant (0.625 g) were pre-mixed in a glass vial and purged with nitrogen for 20 min before transferal into the autoclave with a glass syringe. The CO_2 pressure in the autoclave was first increased to ~6 MPa and the autoclave was then heated to 60 °C whilst the contents were stirred mechanically.[68] The final pressure and temperature were gradually adjusted to ~27 MPa and 65 °C over a period of 15 min. The reaction was carried out for 18 hours to achieve full conversion of the MMA. The second monomer 4VP (5 g) and additional AIBN (6.3 mg) were purged with N_2 for 15 min and added to the autoclave *via* a HPLC pump at 1 ml min^{-1}. The polymerisation of 4VP was then allowed to proceed for 20 h before the autoclave was first cooled down to 25 °C and then depressurised. The product was observed to be an off-white fine free flowing dry powder and was collected for analysis.

2.3 Selective swelling

To introduce porosity to the as-synthesised BCP microparticles, the original BCP microparticles (50 mg) were fully dispersed in alcohol (3 ml) in a glass vial (3.5 ml) and shaken 3 times by hand over a two-hour period. The particles were left standing until they settled to the bottom of the vial. The upper alcohol layer was removed and then hexane (3 ml) was poured into the vial and the particles were fully rinsed by vigorous shaking. The particles were then allowed to resettle before removing the hexane layer after 2 h. The hexane rinse was then repeated three times to completely remove all of the alcohol and then dried in a vacuum oven at 25 °C for >2 h before further analysis.

2.4 Analysis

The block copolymers were characterised by ^{1}H NMR in $CDCl_3$ on a Bruker AV3400 (400 MHz) spectrometer. Gel Permeation Chromatography (GPC) analysis was carried out on an Optilab-rEX (Wyatt) in a mixture of chloroform/ethanol/triethylamine (90/9/1 by volume) for PMMA-*b*-P4VP at a flow rate of 0.5 mL min^{-1} and 25 °C. GPC Columns were composed of K-G, a K-805L and a HT-803 column (Shodex) and calibrated with PMMA narrow standards.

For SEM, the samples were mounted on an aluminium stub and sputter-coated with platinum or iridium prior to imaging on a JEOL 7100F FEG-SEM at accelerating voltage of 2 kV or a FEI Quanta 650 ESEM at 10 kV. The average pore width based on SEM was measured by counting over 100 pores using the commercial software package NanoMeasurer 1.2.5.

Thin sections for cross-sectional TEM were obtained from the original powder BCP microparticle samples by embedding them in an epoxy resin (Agar 100) cured at 55 °C for 2 days. Thin sections (~80 nm) were cut by ultra-microtome using a diamond knife (Leica Diatome Ultra 45°) and were placed on copper TEM grids (Agar). The porous microparticle samples were similarly mounted but were cut by cryo-ultra-microtome. The samples were first placed on the surface of a drop of sucrose solution (5%) on a sample stick following by freezing in liquid nitrogen. The frozen microparticles were then ultra-microtomed into thin sections of ~100 nm at −60 °C using a glass knife. These cross-sections on the copper grids were then imaged using either a JEOL 2100Plus TEM at 200 kV or FEI Tecnai BioTwin-12 TEM at 100 kV at room temperature. PMMA-*b*-P4VP samples were stained with I_2 vapour for ~2 h where stated to enhance the domain contrast in the images. P4VP preferentially absorbs I_2 and appears as dark regions in bright field TEM. The domain sizes in the TEM were measured by counting over 100 domains using the software package NanoMeasurer 1.2.5.

The porosity and surface area of the prepared samples were characterised with a Micromeritics ASAP 2420 instrument by N_2 adsorption at 77 K. Prior to the measurements the samples were first degassed at 70 °C for 16 h. The surface area was calculated by the Brunauer–Emmett–Teller (BET) method using the N_2 adsorption isotherm data within the relative pressure ranging from 0.05 to 0.3. The density functional theory (DFT) method, which is described in detail elsewhere,[69,70] was used to extract the pore size distribution from the adsorption branch using the Micromeritics software. When both mesopores and macropores exist in a material it is necessary to assess the pore width distribution relative to both pore volume and surface area; mesopores contribute to surface area, whilst macropores significantly increase pore volume.

Tilt TEM and tomography. Conventional bright-field TEM of these particles is limited by two factors, first, that the image is a 2-dimensional projection and second, that the sample has to be thin enough to allow at least partial transmission of the electron beam. The complexity of a fully porous 3-dimensional structure is not readily comprehended in a 2-dimensional projection. However, many of the microparticles could be seen to be partially electron transparent even at their thickest points. Since this allows information to be obtained from the entire volume, and the contrast mechanism of conventional bright-field TEM images in these samples is predominantly proportional to volume, tomographic reconstruction from a tilt series was therefore possible.

For an accurate reconstruction, the sample was deposited onto a lacey carbon support TEM grid pre-prepared with 10 nm gold fiducial markers to aid computer alignment. A total of 120 images were manually acquired at 1 degree steps in a single axis tilt series, using a Gatan 916 room temperature tomography holder in a JEOL 2100Plus equipped with a Gatan US1000 CCD camera at 200 kV. Post-acquisition alignment and reconstruction was performed using the IMOD software (http://bio3d.colorado.edu/imod/) utilising the WBP and SIRT reconstructions.

3. Results and discussion

3.1 Fabrication of porous microparticles *via* selective swelling of the minority block

Poly(methyl methacrylate)-*b*-poly(4-vinyl pyridine) (PMMA-*b*-P4VP) (M_n = 56 400 g mol^{-1}; $Đ$ = 1.47), denoted as M-V27.8 (where M represents PMMA, V represents P4VP, and 27.8 represents the molar fraction of P4VP) was synthesised as microparticles *via* RAFT controlled dispersion polymerisation in $scCO_2$. After swelling with ethanol, a selective solvent for P4VP, and rinsing with the non-solvent hexane the particle morphology was clearly porous (Fig. 1a). The SEM image shows open surface pores that are partially interconnected into sub surface cylindrical pores and a deeper pore network, with an average pore width of d_w = 112.7 nm. The subsurface porosity is demonstrated by SEM images at higher magnification (Fig. 1b) where much smaller pores with d_w = 20.3 nm are visible below. TEM images (Fig. 1c) indicate that the porosity persists throughout the entire microparticle. A thin slice (~150 nm) was cut by cryo-ultra-microtome and the TEM images (Fig. 1d) confirm the pores are interconnected and form a bicontinuous porous network.

Prior to ethanol swelling the original M-V27.8 microparticles have a phase separated morphology of spherical P4VP domains in a PMMA matrix (Fig. S1c†). These internal patterns were formed *in situ* by polymerisation induced phase separation.[63] The minority P4VP domains show an average size of d = 21.7 nm (measured from TEM). A distinctive periphery clearly shows larger P4VP domains with d = 60.9 nm (refer to S2† for all TEM-derived domain size measurements). After the solvent swelling interconnected channels are formed and these have an average internal pore width of d_w = 51.1 nm (Fig. 1d), which is twice the original P4VP domain size of d = 21.7 nm and is a result of the P4VP ethanol swelling interaction.

The swelling–deswelling process is best described schematically (Scheme 1). The swelling of these 3D microparticles is

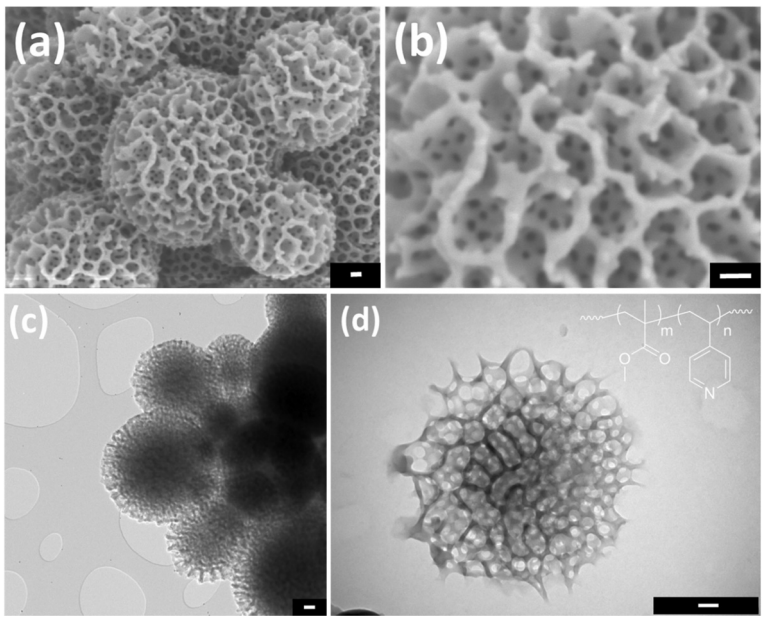

Fig. 1 SEM and TEM images of PMMA-*b*-P4VP (M-V27.8) porous microparticles with pores created by selective swelling in ethanol. (a, b) SEM images of the porous microparticles at different magnification at 2 kV, (c) particle TEM image at 200 kV, (d) cross sectional TEM image of sliced section (~150 nm thickness by cryo-ultra-microtome) without staining and at 100 kV. The inset in (d) is the chemical structure of PMMA-*b*-P4VP. Scale bar represents 100 nm in all cases.

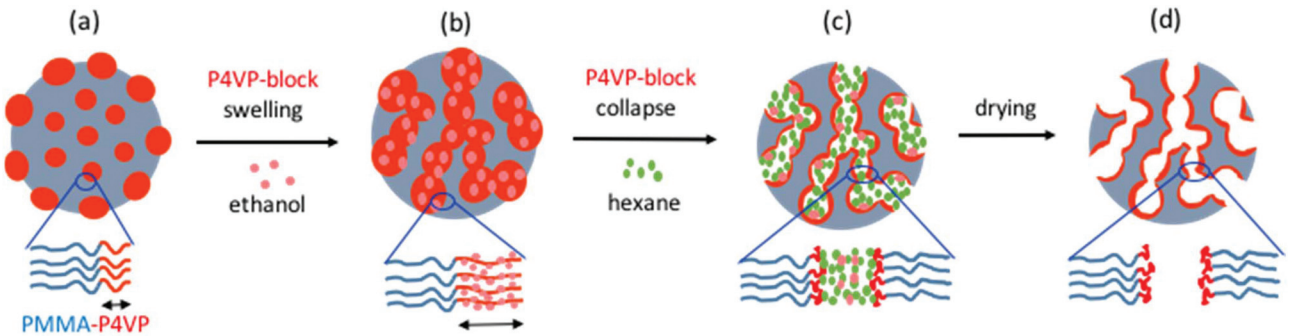

Scheme 1 Schematic demonstration of pore generation throughout BCP microparticles *via* selective solvent swelling induced order-to-order morphology transition and then morphology fixation by fast de-swelling.

somewhat different from 2D thin films,[41,44,51,52] which generally have one-side confined by a solid substrate and the swollen minority chains can only move towards the free surface. In a 3D BCP microparticle system, the selective solvent penetrates and swells the microparticle from all directions and the movement of the swollen chains as well as the plastic deformation of the non-swollen glassy domains occurs symmetrically. Initially, the spherical domains of the minority component P4VP are swollen with the selective solvent ethanol (Scheme 1a). As its volume increases, the minority component pierces through the glassy domains of the majority block PMMA and a bicontinuous morphology evolves (Scheme 1b). Hexane is a poor solvent for both PMMA and P4VP but it is miscible with ethanol. Upon the addition of hexane the swollen minority block collapses (Scheme 1c), but the nanoporous morphology of the partially swollen BCP microparticles is fixed by the rigid, continuous scaffold that is formed by the glassy PMMA. Thus, nanopores with walls consisting of the collapsed minority P4VP blocks are formed in place of the original P4VP domains (Scheme 1d). Furthermore, the collapse of the surface layer, which largely consists of P4VP, leads to the formation of an open nano-porous system at the microparticle surface. Critically, the high T_gs of both blocks and their inertness to air, humidity and (moderate) temperatures ensures that the resulting porous microparticles are stable at ambient conditions indefinitely (Fig. S3†).

3.2 Pore size and shape control

To investigate the effect of the volume fraction of the minority P4VP block on the porosity, we synthesised PMMA-*b*-P4VP

microparticles with similar PMMA chain lengths (*ca.* MW = ~50 kg mol^{-1}) and varied the P4VP chain length to give molar fractions from 9–45 mol% (Table 1, refer to Fig. S4† for the raw GPC data). The smallest P4VP block (2.6 kDa, **M-V9.1**) likely does not phase separate and shows no readily visible structure in the TEM (see Fig. S1e†). However, when the P4VP block is a little longer >13 mol% (**M-V13.3**) the polymeric microparticles show internal phase separation of spherical P4VP domains in a PMMA matrix (TEM mapping of thin sections Fig. S1a†). For larger P4VP blocks, the domain size increases from 12.5 nm to 25.5 nm as the P4VP chain length increases and the P4VP fraction rises from 13.3 mol% to 30.9 mol%. A distinctive periphery layer of large P4VP domains begins to appear very strongly as the P4VP content is increased to 19 mol% (Fig. S1b–d†). These peripheral P4VP domains are enlarged from 57 nm to 106.3 nm at 19.9 and 30.9 mol% P4VP respectively (Fig. S1, 3†).

It appears that the peripheral surface structure is likely a consequence of progressive monomer exclusion towards the interior of the microparticles. Therefore, at the latter stages of polymerisation the P4VP domains at the periphery are swollen with excess 4VP monomer, leading to the much larger domains as compared with the interior. We did kinetic studies of the copolymerization *via* a sampling tap connected to the autoclave as described previously and the corresponding samples were microtomed and investigated by TEM. These images corroborate the 4VP domains become larger at the particle surface towards the latter stages of the reaction (Fig. S5†). This also likely accounts for the slightly broader than expected MW distributions *ca.* 1.4–1.5 (Table 1). GPC analysis was used to exclude the possibility of P4VP homopolymer contamination for each sample. In each case no obvious shoulders were present, and extensive washing with ethanol (a good solvent for P4VP) showed no distinct mass loss or GPC profile changes (see Fig. S6† for M-V27.8).

The BCP microparticles underwent swelling/deswelling as described and SEM images (Fig. 2) show the porous microparticles obtained from PMMA-*b*-P4VP for a range of P4VP molar fractions. At low P4VP fraction (13.3 mol% – sample **M-V13.3**) the images show isolated spherical pores on the particle surface (Fig. 2a and b). These surface pores are arranged in a near hexagonal array. As the molar fraction of P4VP is increased to 19.9 mol% (sample **M-V19.9**), the larger surface open pores partially fuse and where 2 to 4 pores merge, they morph into a short cylindrical surface feature (Fig. 2c and d). This is a direct result of the increased swollen P4VP volume exerting increased pressure on the glassy PMMA matrix, leading to rupturing and merging of isolated spherical P4VP domains. A similar pore structure evolution from spheres to channels was previously observed in the swelling of 1D nanorods at longer swelling times.[46,48] Some interesting pore geometries have also been reported previously by changing the BCP composition and hence the swellable block fraction in large compound micelles or nanospheres.[46,60–62]

When the minority P4VP block is further increased to 27.8 mol% (sample **M-V27.8**) more ethanol absorbs and the swollen P4VP volume increases concomitantly (Fig. 2e and f), giving interconnected open surface pores and a much larger surface pore width, d_w = 112.7 nm (compared to **M-V19.9**, d_w = 74.2 nm). Thus, the original partially merged spherical P4VP domains observed in **M-V19.9** have extended to form a bicontinuous morphology fixed into the glassy PMMA scaffold (Fig. 2e). Increasing the P4VP block further to 30.9 mol% (sample **M-V30.9**) leads to significantly more surface porosity (Fig. 2g and h) where the surface bicontinuous channels now have an average pore width of d_w = 168.8 nm from the SEM. Finally, the sample with a P4VP block ratio of 36.4 mol% (**M-V36.4**) shows a loss of control and collapse of the surface pores (Fig. S9a and b†); Coalescence and fusion leads to less well-defined pores because there is insufficient glassy PMMA present to stabilise and fix the swelling induced morphology.

The SEM images also hint at sub-surface pores of the order d_w = 20–25 nm (Fig. 2); to probe these, the same samples were further characterised by TEM imaging (Fig. 3). For **M-V13.3b**,

Table 1 Characterisation of the PMMA-b-P4VP block copolymers synthesised *via* RAFT dispersion polymerisation in $scCO_2$

Entries		NMR	GPC[a]				M_n by ^{1}H NMR[b]	
			1st block PMMA		BCPs		P4VP	BCPs
M-V*x*[c]	Target M_n (g mol^{-1})	Molar ratio[d]	M_n	$Đ$	M_n	$Đ$	M'_n	M'_n
M-V9.1	50k/2.6k	90.9/9.1	48 500	1.26	52 000	1.52	5100	53 600
M-V13.3	50k/5.6k	86.7/13.3	39 000	1.25	51 100	1.43	6300	45 300
M-V19.9	50k/15k	80.1/19.9	41 300	1.23	58 500	1.44	10 800	52 100
M-V27.8	50k/17k	72.2/27.8	—	—	56 400	1.47	—	—
M-V30.9	50K/20K	69.1/30.9	40 400	1.24	59 400	1.50	19 000	59 400
M-V36.4	50k/25k	63.6/36.4	—	—	58 900	1.80	—	—
M-V36.9	200k/133k	63.1/36.9	119 300	1.83	153 100	2.24	73 300	192 600

[a] Mixed solvent of $CHCl_3$ + ethanol + TEA (90 : 10 : 1, v/v/v) as eluent and PMMA as calibration standards. [b] M_n is the MW calculation based on both ^{1}H NMR (block ratio) and GPC (the M_n of 1st block PMMA); $M'_n(\text{P4VP}) = \frac{\text{P4VP(mol)}}{\text{PMMA(mol)}} \times \frac{105.1}{100.1} \times M_{n\,GPC}^{PMMA}$; $M'_n(\text{BCPs}) = M'^{PMM}_{nGPC} + M'_n(\text{P4VP})$. [c] M, V, and the numerals after V denote PMMA, P4VP, and the molar fraction of P4VP block, respectively. [d] Molar ratio of PMMA/P4VP; for entries M-V27.8 and M-V36.4 the 1st block was not sampled before adding 4VP to the autoclave.

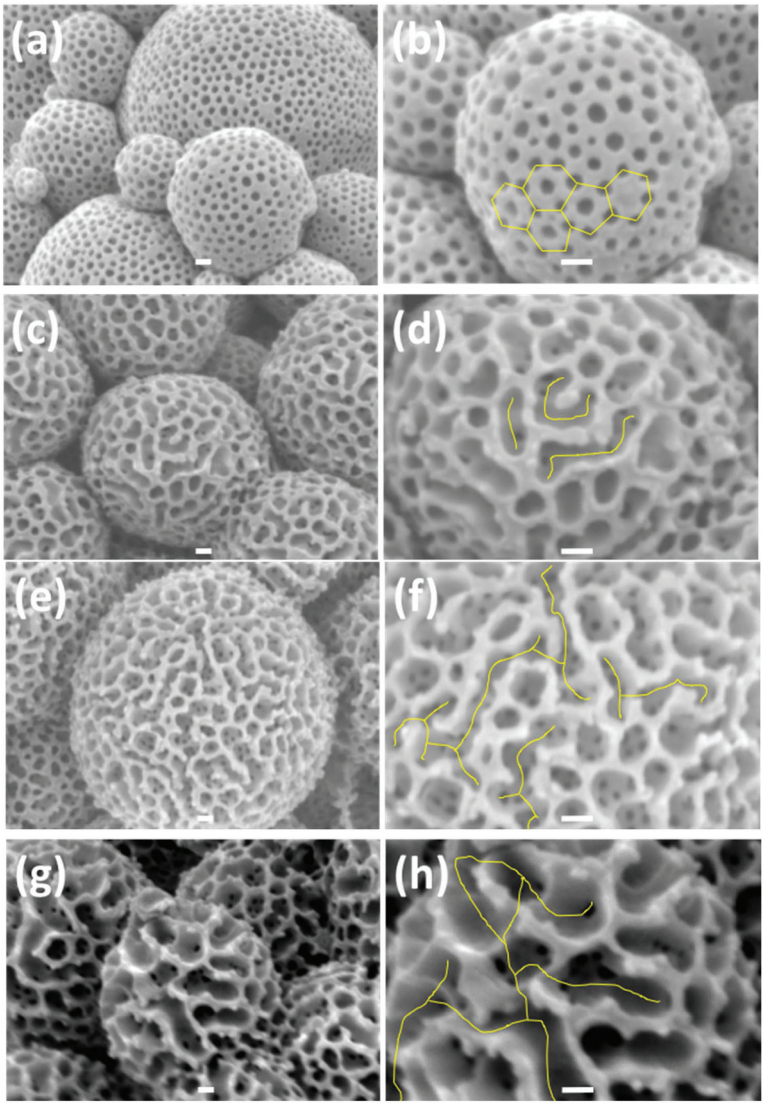

Fig. 2 Controlled nanoporosity introduced into block copolymer microparticles by selective swelling/deswelling in ethanol with hexane. SEM images of PMMA-*b*-P4VP porous microparticles. (a) M-V13.3, (c) M-V19.9, (e) M-V27.8, (g) M-V30.9. (b, d, f, h) are higher magnification images of (a, c, e, g) respectively. Scale bar in all cases is 100 nm. The yellow lines in (b, d, f, h) mark the surface pore evolution from isolated spherical pores to short channels, and to interconnected channels. The original BCP particles are shown in Fig. S11.†

the pores only develop near the surface and not throughout the whole particle (Fig. 3a).

At higher P4VP content >19 mol%, the TEM data clearly demonstrate that the microparticles are highly porous throughout (Fig. 3b–d) and confirm that ethanol diffuses effectively through the glassy PMMA regions, the major component of the BCP microparticles.

We hypothesised that the swelling process for the 3D microparticles is time-dependent. Wang *et al*. investigated 1D nanorods of PS-*b*-P2VP with ethanol and found that varied pore morphologies were achieved by increasing swelling time from 10 min to 66 h.[46,54] However, they began with just a very dilute suspension of nanorods in ethanol and argued that the swelling at 20 °C was tiny. In our study, the BCP microparticles are a dry powder and we have a much greater material bulk. We found that a substantial time *ca.* >1 h was required just to fully suspend the BCP microparticle powder in ethanol, whereas for full solvent penetration, >12 h was required to fully swell gram quantities of our microparticles.

Tilt TEM tomography. To further demonstrate the internal porosity, a 3D structural analysis of the pores throughout a whole microparticle was undertaken using tilt TEM imaging with angles of up to 120°. The particles initially displayed a very small shrinkage of 2–2.5% in diameter but then quickly stabilised under the conditions of the measurements being made. A certain level of radiation damage is to be expected upon extended exposure of the soft polymers to the electron beam,[71] but it is clear that the lacy carbon film coated on the TEM grid was sufficient at dissipating the charge on the microparticles.

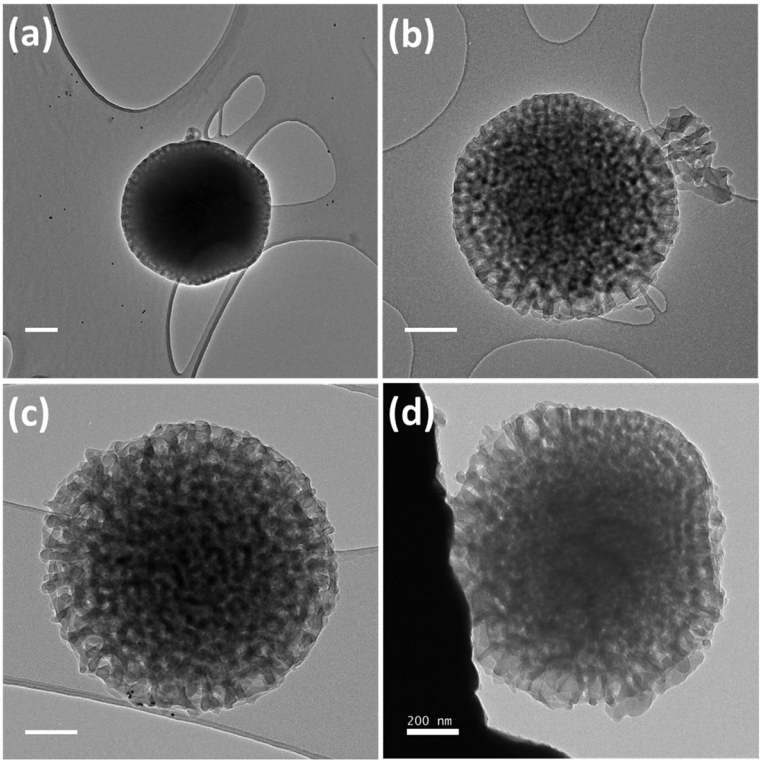

Fig. 3 TEM bright-view images of PMMA-*b*-P4VP porous microparticles with varied P4VP molar fraction. (a) M-V13.3, (b) M-V19.9, (c) M-V27.8, (d) M-V30.9. TEM images show that porosity has penetrated through the whole particle in b, c, d. Scale bar represents 200 nm.

Pore size measurements throughout the sample were made from the tomographic reconstruction in the *Z*-axis (*i.e.* parallel with the original zero tilt image) to minimise distortion due to the missing wedge. Eight image slices (Fig. 4) for sample M-V30.9 reveal the pore structure. Reconstructed slices at the surface of the structure (Fig. 4, image 001, 021) reveal large open pores (d_w = 70.8 nm). Slices in the middle of the reconstruction (passing though the centre of the microparticle) reveal much smaller pore widths at the particle centre (d_w = 24.4 nm, image 141 in Fig. 4). All slices show the nanopore structures, which further confirm that the pores are developed throughout the particle. The tilt series of images was then

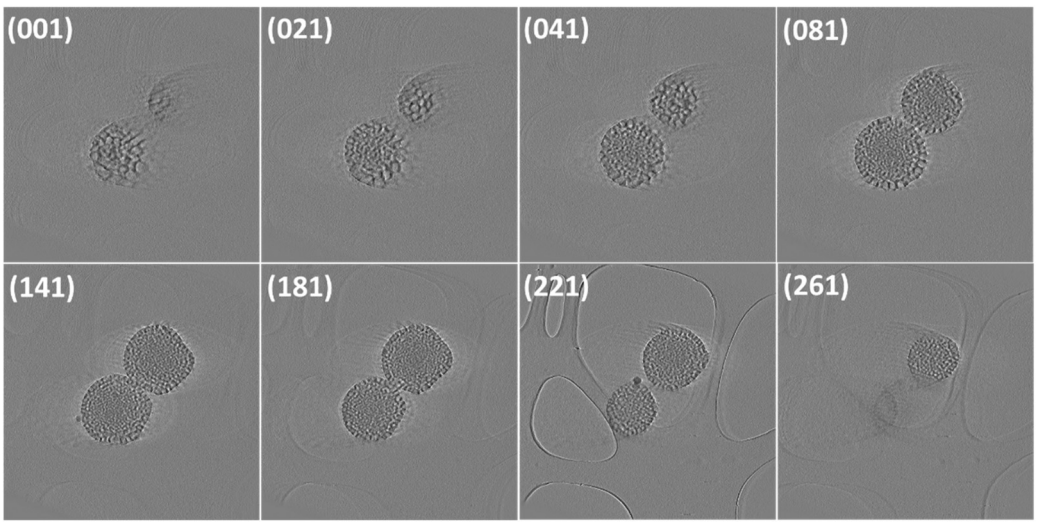

Fig. 4 A selection of slices from the SIRT tomographic reconstruction of a porous microparticle (M-V30.9) showing 8 of the 280 slices from the top surface to the bottom and the supporting carbon film. The tilt series was taken at a 2550 electrons per nm^2 per s dose rate with an 18 min and 41 s acquisition time.

combined to form a video for each BCP sample with a different mol% of P4VP (see illustrative videos in ESI†). At low P4VP fraction (**M-V13.3**) isolated spherical pores have developed near the surface layers but the bulk appears to be non-porous (Fig. S7a†). However, as the P4VP fraction increases it is clear that high quality internal porosity evolves with very clear interconnectivity throughout the entire particle (Fig. S7b–d†).

The porous materials were further investigated using nitrogen adsorption isotherms (BET measurement at −196 °C, Fig. 5). The majority of the isotherms were typical type IV, characterised by the dominance of the H1 hysteresis loops observed at high relative pressures (P/P^0) region. The adsorption capacity of nitrogen was negligible for virtually all the samples analysed at relative pressures up to 0.8 indicating that the materials are essentially purely mesoporous but containing some macropores. At low P4VP content, **M-V13.3** presents a characteristic H2(b) loop, usually associated with "ink-bottle like" pores. But the porosity in this sample is quite low and consistent with the TEM/tilt TEM observations which reveal mesopores only in the sub-surface layers with pore width 21.2 nm (Fig. 3a and Fig. S8a†).

The other samples show greater porosity and pore size distributions (Fig. 5b and c) indicating that at higher mole ratios of P4VP there are multiple regular peaks of meso- and macropores centred at 25.2, 37.0, 50.3, 68.4, 86.2 and 117.2 nm. Such pore size distributions have previously only been observed for siliceous mesocellular foams with interconnected 3D pore cell structures, which can only be prepared by cumbersome hydrothermal templating methods under well-regulated and time-consuming conditions.[72,73] The characteristic surface textural properties of our materials appear to be dictated by the P4VP-block content, suggesting that the unique regular interconnected 3D porous structures do originate from the geometric configurations of the block copolymer internal structures. TEM and Tilt TEM data again support our observations of surface and internal pores merging into longer channels and then interconnected pores (Fig. 3 and 4).

The presence of micropores in these samples is small compared to the large population of meso- and macropores (Fig. S12†). As a result, the specific BET surface areas of these materials are generally limited, ranging from 11 to 91 $m^2\ g^{-1}$ but with total pore volumes approaching up to 0.69 $cm^3\ g^{-1}$. However, what is clear is that the surface area and pore volume both increase significantly with increasing P4VP-content, demonstrating that this is the pore-generating domain during the swelling/de-swelling process.

3.3 Pore size control by MW of BCP

The size of the nanodomains formed *via* phase separation of the block copolymers is determined by the constituent block size, where the domain size is proportional to N^x, with N denoting the repeating unit and $x < 1$.[29,74] Here we demonstrate that RAFT controlled dispersion polymerisation in $scCO_2$ can be utilised to achieve higher molecular weight blocks up to 330 kDa (see Table 1). As expected, these much higher molecular weights lead to much larger domain sizes, with d(P4VP)

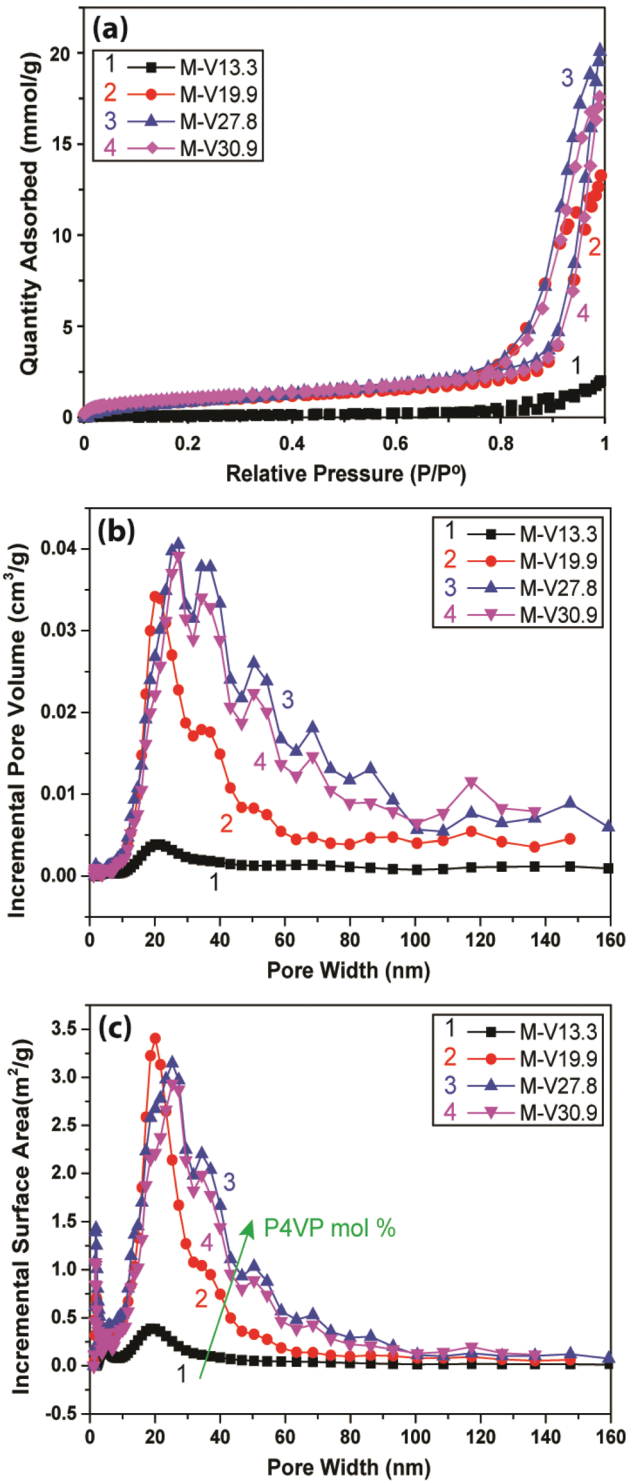

Fig. 5 Nitrogen adsorption analysis of porous microparticles. (a) Hysteresis loop of quantity adsorbed *versus* relative pressure; (b) DFT pore volume distribution; and (c) DFT surface area distribution.

increasing from 25.5 nm to 60.4 nm as we progress from **M-V30.9** (MW = 59 400 g mol^{-1}) to the much larger **M-V36.9** (MW = 153 100 g mol^{-1}) (the as-synthesised domains are shown in Fig. S10†). The swelling process for **M-V36.9** yielded

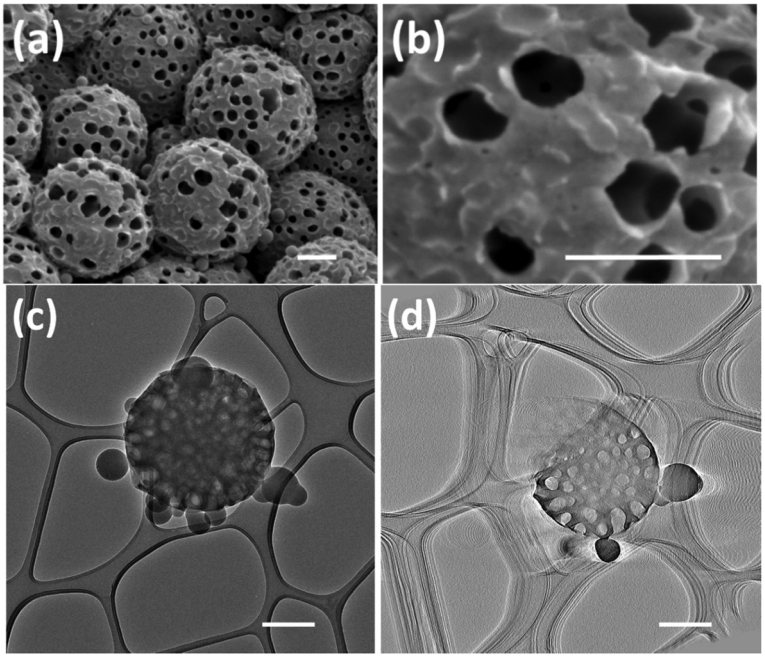

Fig. 6 High molecular weight PMMA-*b*-P4VP porous microparticles M-V36.9 with block sizes targeted at 200k–133k. (a, b) SEM images at different magnification; (c) bright-field TEM image and (d) a slice through the centre of the sample from a tomographic reconstruction (accelerating voltage of 200 kV; WBP reconstruction, no fiducial markers). Scale bar 500 nm in each case.

porous microparticles with isolated large pores at the particle surface (average pore width d_w = 168.9 nm) (Fig. 6). A TEM/tilt TEM video (Fig. S7e†) clearly shows that the pores are interconnected and that these large pores are found at both the particle surface and internally (Fig. 6c). The absence of interparticle fusion for this system when compared with M-V36.4 (50k–25k) is attributed to the significantly reduced solubility of the P4VP block in ethanol as the molecular weight increases. Tomographic images based on the tilt TEM series show internal porosity (Fig. 6d) and demonstrate that the pore size can be controlled and extended to larger macropores of up to ~200 nm by increasing the MW of the blocks, and hence also

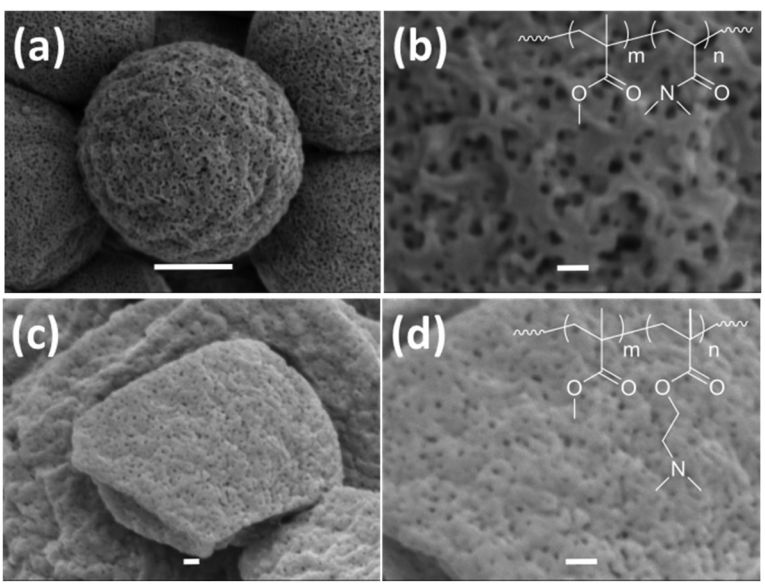

Fig. 7 SEM images of PMMA-*b*-PDMA swollen with ethanol (a, b) and PMMA-*b*-PDMEAMA swollen with methanol (c, d) porous microparticles created by selective swelling in ethanol. (a, b) M-DMA20.2, (c, d) M-DMAEMA11.8. The inserts in (b, d) show the chemical structure of PMMA-*b*-PDMA and PMMA-*b*-PDMEAMA, respectively. Scale bar is 1000 nm in (a) and 100 nm in (b–d).

increasing the domain size and the available volume for ethanol swelling. Such large macropores cannot easily be achieved by conventional routes such as UV etching, ozonolysis, hydrolysis, or complexation with additives, which generally lead to much smaller mesopores <50 nm.[25] In those methods the pore size is limited to the domain size of the intrinsic BCP self-assembled nanostructure, which is usually in the range of 10–100 nm. By contrast, our approach using swelling induced order-to-order morphology transitions and morphology reconstruction by fast de-swelling can facilitate significantly larger features.

3.4 Other block copolymer systems

The same selective solvent swelling and fast de-swelling process was applied to a range of other microparticulate block copolymers. The key was to determine the most appropriate selective swelling solvent and de-swelling pair for other systems (Fig. 7) based upon PMMA-*b*-PDMA (20.2 mol% PDMA, **M-DMA20.2**), and PMMA-*b*-PDMAEMA (11.8 mol% PDMAEMA, **M-DMAEMA11.8**). The polymers were again synthesised *via* RAFT controlled dispersion polymerisation and treated with alcohols as a selective swelling solvent for the minority PDMA and PDMAEMA blocks and then hexane for de-swelling. The microparticulate morphology was well conserved for **M-DMA20.2** (Fig. 7a and b) when swollen with ethanol compared to the original (Fig. S11g†). The particles also developed surface open pores (d_w = 26 nm) which appear interconnected. In contrast, swelling **M-DMAEMA11.8** with ethanol causes inter-particle fusion (Fig. S13†). A lower alcohol of methanol was found to significantly reduce the particle fusion for **M-DMAEMA11.8** (Fig. 7c and d). Surface open pores developed, but these were much smaller d_w = 12 nm. This illustrates that it is key to find the appropriate selective swelling solvent when changing the BCP system, by considering the solubility parameters of the swelling block/swelling solvent to achieve the optimal porous structures. The successful fabrication of nanoporous particles from PMMA-*b*-PDMA and PMMA-*b*-PDMAEMA highlights the versatility of our approach and could likely be applied to a very wide range of block copolymer systems to achieve nanoporous soft materials with bespoke surface functionality.

4. Conclusions

We present a new methodology for creating controlled nanoporous block copolymer microparticles by synthesis in $scCO_2$ followed by a swelling/rapid de-swelling route. Our use of a versatile RAFT controlled dispersion polymerisation in $scCO_2$ allows excellent control of block lengths up to 330 kDa. Thus, we present fine control of the domain sizes in the BCP microparticles to provide a wide range of nanopore sizes and shapes. Increasing the length of the swellable block increases the swollen block volume and induces order-to-order morphology transitions in the swollen state. After rapid de-swelling the resultant porosity shows a range of morphologies from isolated spheres through to short channels and interconnected networks; leading to unprecedentedly large pores ~200 nm. Innovative use of tilt-TEM microtomography has allowed us to probe in detail the structure of the porosity in the microparticles and to demonstrate definitively that the porosity persists throughout these larger 3-D structures. The method was also extended to a broader range of functional polymers including PMMA-*b*-P4VP, PMMA-*b*-PDMA, and PMMA-*b*-PDMEAMA. Both the BCP microparticle synthesis and the swelling/rapid deswelling process have been demonstrated on the multigram scale and could easily be scaled to produce kilogram quantities. Thus, we have presented a facile, versatile and therefore practical strategy for the bespoke fabrication of hierarchically macro- and mesoporous block copolymer microparticles, with significant promise for use in a wide range of potential applications.

Conflicts of interest

There are no conflicts to declare.

Acknowledgements

We are grateful to the Leverhulme Trust (RPG-2014-034) for their support of this project (GH and TMB). MA is deeply grateful to the UNNES-IDB scholarship for a PhD Scholarship to Nottingham. STS is grateful to the Erasmus + scheme for the award of a higher education traineeship to support his visit to Nottingham. We thank the University of Nottingham and in particular the invaluable technical support received from our high pressure workshop technicians Richard Wilson, Peter Fields and Martin Dellar. Our research made use of the excellent electron microscopy facilities in the Nano-Micro Research Centre (NMRC) in the University of Nottingham in particular the 2100Plus TEM is supported by the EPSRC [EP/L022494/1]. We thank also Nicola Weston for the assistance in electron microscopies. We thank Yaoming Zhang for the valuable discussion/suggestions on P4VP and Prof. Ullrich Steiner for his input on block copolymer materials.

References

1 P. Barbaro and F. Liguori, *Chem. Rev.*, 2009, **109**, 515–529.
2 D. C. Sherrington, *J. Polym. Sci., Part A: Polym. Chem.*, 2001, **39**, 2364–2377.
3 R. Say, S. Emir, B. Garipcan, S. L. Patir and A. Denizli, *Adv. Polym. Technol.*, 2003, **22**, 355–364.
4 A. R. Bogdan, B. P. Mason, K. T. Sylvester and D. T. McQuade, *Angew. Chem., Int. Ed.*, 2007, **46**, 1698–1701.
5 J. Lu and P. H. Toy, *Chem. Rev.*, 2009, **109**, 815–838.
6 M. R. Buchmeiser, *Chem. Rev.*, 2009, **109**, 303–321.
7 J. Deng, Y. Yu, S. Dun and W. Yang, *J. Phys. Chem. B*, 2010, **114**, 2593–2601.

8 M. J. Benes, D. Horak and F. Svec, *J. Sep. Sci.*, 2005, **28**, 1855–1875.
9 J. Haginaka, *J. Chromatogr. B: Anal. Technol. Biomed. Life Sci.*, 2008, **866**, 3–13.
10 A. Basso, P. Braiuca, L. De Martin, C. Ebert, L. Gardossi, P. Linda, S. Verdelli and A. Tam, *Chemistry*, 2004, **10**, 1007–1013.
11 L. Sinigoi, P. Bravin, C. Ebert, N. D'Amelio, L. Vaccari, L. Ciccarelli, S. Cantone, A. Basso and L. Gardossi, *J. Comb. Chem.*, 2009, **11**, 835–845.
12 S. Mei, C. J. Jafta, I. Lauermann, Q. Ran, M. Kärgell, M. Ballauff and Y. Lu, *Adv. Funct. Mater.*, 2017, 27.
13 L. Wang, S. Mei and Z. Jin, *Macromol. Chem. Phys.*, 2013, **214**, 2579–2583.
14 A. Stein, *Adv. Mater.*, 2003, **15**, 763–775.
15 I. Tokarev and S. Minko, *Adv. Mater.*, 2010, **22**, 3446–3462.
16 D. L. Elbert, *Acta Biomater.*, 2011, **7**, 31–56.
17 M. I. J. Stich, M. Schaeferling and O. S. Wolfbeis, *Adv. Mater.*, 2009, **21**, 2216–2220.
18 A. Salinas-Castillo, M. Camprubi-Robles and R. Mallavia, *Chem. Commun.*, 2010, **46**, 1263–1265.
19 Y. Lan, L. Yang, M. Zhang, W. Zhang and S. Wang, *ACS Appl. Mater. Interfaces*, 2010, **2**, 127–133.
20 Y. Jiang, Q. Sun, L. Zhang and Z. Jiang, *J. Mater. Chem.*, 2009, 19.
21 V. Rastogi, K. P. Velikov and O. D. Velev, *Phys. Chem. Chem. Phys.*, 2010, **12**, 11975–11983.
22 M. T. Gokmen and F. E. Du Prez, *Prog. Polym. Sci.*, 2012, **37**, 365–405.
23 S. Guo, J. Rzayev, T. S. Bailey, A. S. Zalusky, R. Olayo-Valles and M. A. Hillmyer, *Chem. Mater.*, 2006, **18**, 1719–1721.
24 J. Bang, S. H. Kim, E. Drockenmuller, M. J. Misner, T. P. Russell and C. J. Hawker, *J. Am. Chem. Soc.*, 2006, **128**, 7622–7629.
25 D. Wu, F. Xu, B. Sun, R. Fu, H. He and K. Matyjaszewski, *Chem. Rev.*, 2012, **112**, 3959–4015.
26 Y. Mai and A. Eisenberg, *Chem. Soc. Rev.*, 2012, **41**, 5969–5985.
27 H. Y. Hsueh, C. T. Yao and R. M. Ho, *Chem. Soc. Rev.*, 2015, **44**, 1974–2018.
28 S. W. Robbins, P. A. Beaucage, H. Sai, K. W. Tan, J. G. Werner, J. P. Sethna, F. J. DiSalvo, S. M. Gruner, R. B. Van Dover and U. Wiesner, *Sci. Adv.*, 2016, **2**, e1501119.
29 F. S. Bates and G. H. Fredrickson, *Annu. Rev. Phys. Chem.*, 1990, **41**, 525–557.
30 I. W. Hamley, *Prog. Polym. Sci.*, 2009, **34**, 1161–1210.
31 N. A. Lynd, A. J. Meuler and M. A. Hillmyer, *Prog. Polym. Sci.*, 2008, **33**, 875–893.
32 V. Abetz and P. F. W. Simon, Phase Behaviour and Morphologies of Block Copolymers, in *Block Copolymers I*, ed. V. Abetz, Springer Berlin Heidelberg, Berlin, Heidelberg, 2005, pp. 125–212.
33 J. S. Lee, A. Hirao and S. Nakahama, *Macromolecules*, 1988, **21**, 274–276.
34 K. Bandyopadhyay, E. Tan, L. Ho, S. Bundick, S. M. Baker and A. Niemz, *Langmuir*, 2006, **22**, 4978–4984.
35 G. D. Fu, Z. Yuan, E. T. Kang, K. G. Neoh, D. M. Lai and A. C. H. Huan, *Adv. Funct. Mater.*, 2005, **15**, 315–322.
36 J. L. Hedrick, K. R. Carter, J. W. Labadie, R. D. Miller, W. Volksen, C. J. Hawker, D. Y. Yoon, T. P. Russell, J. E. McGrath and R. M. Briber, *Adv. Polym. Sci.*, 1999, **141**, 1–43.
37 C.-M. Chung, J.-H. Lee, S.-Y. Cho, J.-G. Kim and S.-Y. Moon, *J. Appl. Polym. Sci.*, 2006, **101**, 532–538.
38 S.-Y. Lu, C.-H. Chang, C.-H. Yu, H.-L. Chen and Y. H. Lo, *J. Mater. Res.*, 2011, **20**, 1523–1528.
39 R. Olayo-Valles, S. Guo, M. S. Lund, C. Leighton and M. A. Hillmyer, *Macromolecules*, 2005, **38**, 10101–10108.
40 Y. Boontongkong and R. E. Cohen, *Macromolecules*, 2002, **35**, 3647–3652.
41 C. Xu, X. Fu, M. Fryd, S. Xu, B. B. Wayland, K. I. Winey and R. J. Composto, *Nano Lett.*, 2006, **6**, 282–287.
42 C. Xu, B. B. Wayland, M. Fryd, K. I. Winey and R. J. Composto, *Macromolecules*, 2006, **39**, 6063–6070.
43 H. Cho, H. Park, T. P. Russell and S. Park, *J. Mater. Chem.*, 2010, 20.
44 U. Zettl, A. Knoll and L. Tsarkova, *Langmuir*, 2010, **26**, 6610–6617.
45 L. Wang, F. Montagne, P. Hoffmann and R. Pugin, *Chem. Commun.*, 2009, 3798–3800.
46 Y. Wang, L. Tong and M. Steinhart, *ACS Nano*, 2011, **5**, 1928–1938.
47 J. Chai and J. M. Buriak, *ACS Nano*, 2008, **2**, 489–501.
48 Y. Wang, U. Gösele and M. Steinhart, *Nano Lett.*, 2008, **8**, 3548–3553.
49 S. Park, J. Y. Wang, B. Kim and T. P. Russell, *Nano Lett.*, 2008, **8**, 1667–1672.
50 W. Hwang, M.-H. Ham, B.-H. Sohn, J. Huh, Y. S. Kang, W. Jeong, J.-M. Myoung and C. Park, *Nanotechnology*, 2005, **16**, 2897–2902.
51 S. Park, J.-Y. Wang, B. Kim, J. Xu and T. P. Russell, *ACS Nano*, 2008, **2**, 766–772.
52 Z. Chen, C. He, F. Li, L. Tong, X. Liao and Y. Wang, *Langmuir*, 2010, **26**, 8869–8874.
53 J.-T. Chen, M. Zhang, L. Yang, M. Collins, J. Parks, A. Avallone and T. P. Russell, *J. Polym. Sci., Part B: Polym. Phys.*, 2007, **45**, 2912–2917.
54 Y. Wang, U. Gosele and M. Steinhart, *Nano Lett.*, 2008, **8**, 3548–3553.
55 Y. Wang, Y. Qin, A. Berger, E. Yau, C. He, L. Zhang, U. Gösele, M. Knez and M. Steinhart, *Adv. Mater.*, 2009, **21**, 2763–2766.
56 S. Mei, X. Feng and Z. Jin, *Soft Matter*, 2013, **9**, 945–951.
57 C.-W. Chang, M.-H. Chi, H.-W. Ko, C.-W. Chu, Z.-X. Fang, Y.-H. Tu and J.-T. Chen, *Polym. Chem.*, 2017, **8**, 3399–3404.
58 J. Yin, X. Yao, J. Y. Liou, W. Sun, Y. S. Sun and Y. Wang, *ACS Nano*, 2013, **7**, 9961–9974.
59 Y. Wang, *Acc. Chem. Res.*, 2016, **49**, 1401–1408.
60 S. Mei and Z. Jin, *Small*, 2013, **9**, 322–329.
61 H. Fan and Z. Jin, *Macromolecules*, 2014, **47**, 2674–2681.

62 K. H. Ku, J. M. Shin, D. Klinger, S. G. Jang, R. C. Hayward, C. J. Hawker and B. J. Kim, *ACS Nano*, 2016, **10**, 5243–5251.
63 J. Jennings, M. Beija, A. P. Richez, S. D. Cooper, P. E. Mignot, K. J. Thurecht, K. S. Jack and S. M. Howdle, *J. Am. Chem. Soc.*, 2012, **134**, 4772–4781.
64 J. Jennings, M. Beija, J. T. Kennon, H. Willcock, R. K. O'Reilly, S. Rimmer and S. M. Howdle, *Macromolecules*, 2013, **46**, 6843–6851.
65 J. Jennings, S. P. Bassett, D. Hermida-Merino, G. Portale, W. Bras, L. Knight, J. J. Titman, T. Higuchi, H. Jinnai and S. M. Howdle, *Polym. Chem.*, 2016, **7**, 905–916.
66 T. D. McAllister, L. D. Farrand and S. M. Howdle, *Macromol. Chem. Phys.*, 2016, **217**, 2294–2301.
67 J. T. Lai, D. Filla and R. Shea, *Macromolecules*, 2002, **35**, 6754–6756.
68 A. M. Gregory, K. J. Thurecht and S. M. Howdle, *Macromolecules*, 2008, **41**, 1215–1222.
69 Y. Ren, Z. Ma, R. E. Morris, Z. Liu, F. Jiao, S. Dai and P. G. Bruce, *Nat. Commun.*, 2013, **4**, 2015.
70 J. P. Olivier, *Carbon*, 1998, **36**, 1469–1472.
71 R. F. Egerton, P. Li and M. Malac, *Micron*, 2004, **35**, 399–409.
72 P. Schmidt-Winkel, W. W. Lukens, D. Zhao, P. Yang, B. F. Chmelka and G. D. Stucky, *J. Am. Chem. Soc.*, 1999, **121**, 254–255.
73 P. Schmidt-Winkel, W. W. Lukens, P. Yang, D. I. Margolese, J. S. Lettow, J. Y. Ying and G. D. Stucky, *Chem. Mater.*, 2000, **12**, 686–696.
74 I. W. Hamley, *The Physics of Block Copolymers*, Oxford University Press, 1998.

Polymer Chemistry

COUNTRY

United Kingdom

Universities and research institutions in United Kingdom

Media Ranking in United Kingdom

SUBJECT AREA AND CATEGORY

Biochemistry, Genetics and Molecular Biology
Biochemistry

Chemical Engineering
Bioengineering

Chemistry
Organic Chemistry

Engineering
Biomedical Engineering

Materials Science
Polymers and Plastics

PUBLISHER

Royal Society of Chemistry

H-INDEX

127

PUBLICATION TYPE

Journals

ISSN

17599954, 17599962

COVERAGE

2010-2021

INFORMATION

Homepage

How to publish in this journal

SCOPE

Our broad scope includes: -novel synthetic and polymerization methods -renewable polymer synthesis -advanced characterization of polymers -macromolecular structure and function -synthesis and application of novel polymers -reactions and chemistry of polymers -supramolecular polymers -polymerization mechanisms and kinetics -higher-order polymer structures -structure-property relationships of polymers

Join the conversation about this journal

Quartiles

FIND SIMILAR JOURNALS

1
Journal of Polymer Science, Part A: Polymer Chemistry
USA
94%
similarity

2
Macromolecular Rapid Communications
DEU
89%
similarity

3
ACS Macro Letters
USA
88%
similarity

4
Macromolec and Physics
DEU
8
s

SJR

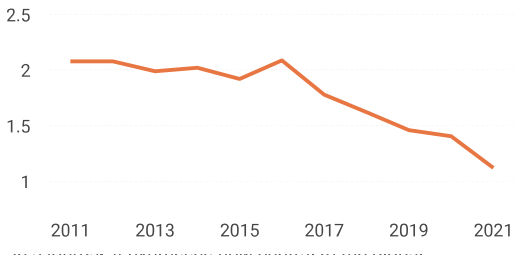

Total Documents

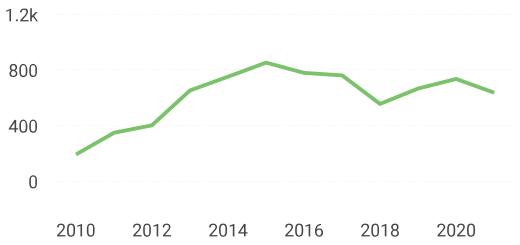

Total Cites Self-Cites

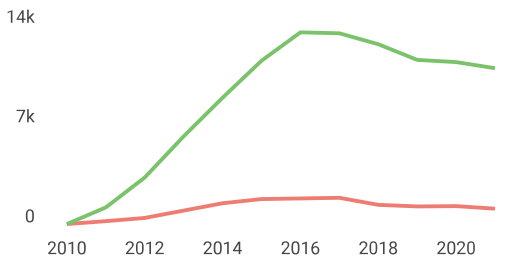

Citations per document

External Cites per Doc Cites per Doc

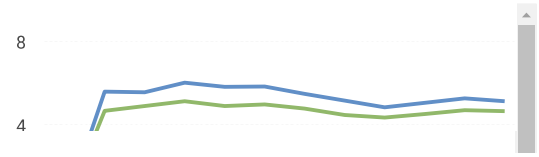

% International Collaboration

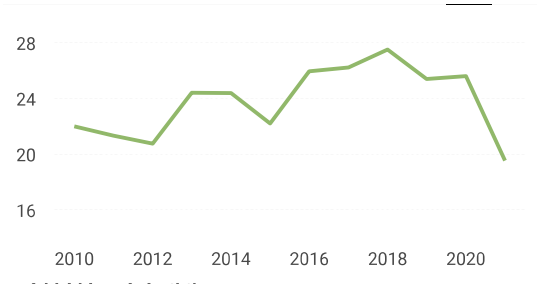

Citable documents Non-citable documents

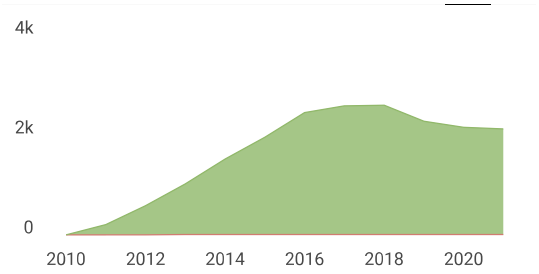

Cited documents Uncited documents

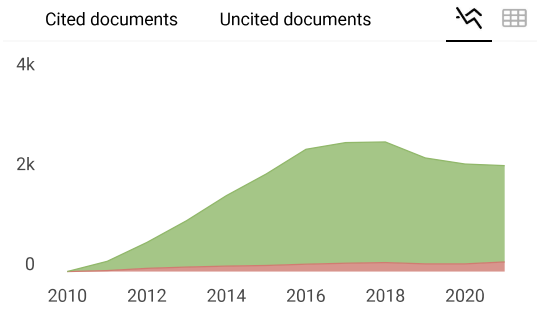

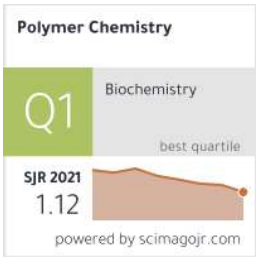

← Show this widget in your own website

Just copy the code below and paste within your html code:

```
<a href="https://w
```

SCImago Graphica

Explore, visually communicate and make sense of data with our **new data visualization tool**.

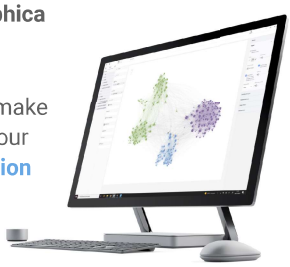

Metrics based on Scopus® data as of April 2022

D **Daisy Auden** 3 years ago

First of all, we are very thankful for your article. It is very happy to share the feelings that your article is very helpful to people to gain knowledge in the field of Chemistry. We suggest you go through our article where it also helps you as well as others.

reply

SCImago Team

Melanie Ortiz 3 years ago

Dear Daisy, thanks for your participation! Best Regards, SCImago Team